Electronic Supplementary Material (ESI) for Physical Chemistry Chemical Physics

ELECTRONIC SUPLEMENTARY INFORMATION

"Insights from impedance spectroscopy into mechanism of thermal decomposition of $M(NH_2BH_3)$ M=H, Li, Na, $Li_{0.5}Na_{0.5}$ hydrogen stores"

Karol J. Fijalkowski, Rafał Jurczakowski, Wiktor Koźmiński and Wojciech Grochala

Contents

1. Synthesis of alkali metal amidoboranes:

We used LiH, NaH, $LiNH_2$ (all 95%, Sigma Aldrich) and NH_3BH_3 of the highest commercially available purity (98%, JSC Aviabor). We sythesized alkali metal amidoboranes in a dry mechanochemical way described in the literature, using tungsten carbide disk milling vessel together with a high energy mill from Testchem. All operations were carried out under argon atmosphere with no contact with atmospheric air, according to the reaction equations:

$LiNH_2 + NH_3BH_3 \rightarrow LiNH_2BH_3 + NH_3\uparrow$
$NaH + NH_3BH_3 \rightarrow NaNH_2BH_3 + H_2\uparrow$
$LiH + NaH + 2NH_3BH_3 \rightarrow NaLi(NH_2BH_3)_2 + 2H_2\uparrow$

Milling was carried out with 5 minutes breaks to avoid thermal decomposition of the product during milling. Regimes of milling are shown below:

$NaNH_2BH_3$	3 times per 1 minute milling
$LiNH_2BH_3$	2 times per 3 minutes of milling
$NaLi(NH_2BH_3)_2$	3 times per 3 minutes of milling

Different milling regimes for different amidoboranes reflect optimization of the milling process due to stability differences of the products.

Since our previous paper (Ref.8) was published, we have improved method of synthesis NaAB (milling procedure contains longer breaks for cooling, or even it is performed at cryogenic LN2 conditions to minimize both thermal decomposition as well as transition to the ionic phase). We have also changed the TGA/DSC/MS procedure which now is much more accurate (the measurement commences at –10°C to get very stable signals from 20°C upwards).

2. IS data at elevated temperature

Imaginary part of electric modulus, *M*'', vs. logarithm of frequency exhibits a distinct peak, which is shifted toward higher frequency as the temperature is raised (cf. Fig.S2.1). The position of this peak nearly coincides with that for the imaginary part of impedance, *Z* '' (Fig.S2.2), and both are clearly separated from the characteristic frequency of dissipation factor, tan(*δ*) (Fig. S2.2). This type of behavior is typical for long range conductivity [R. Gerhardt, J. Phys. Chem. Solids, 55 (1994) 1491-1506].

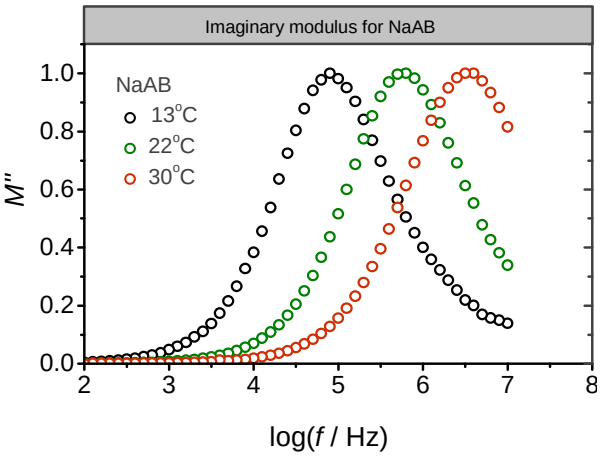

Fig. S2.1. Imaginary part of electric modulus *M*'' normalized to peak for sodium amidoborane at different temperatures.

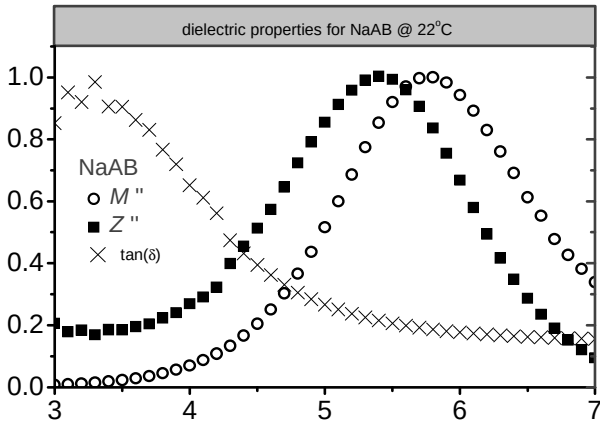

Fig. S2.2. The nearly overlapping peaks of the imaginary part of electric modulus *M*'' and imaginary part of impedance *Z*'' vs. frequency with an accompanying tan*δ* indicating that the conductivity is of a long range nature. Data for sodium amidoborane at 22°C.

3. Powder EIS isothermal scans for NaAB at 38°C, 48°C and 65°C:

We observe growth (followed by shallow decrease) of conductivity of amidoborane samples during isothermal measurements at room or at elevated temperatures. Experiments performed at different temperatures (38°C, 48°C, 65°C) indicate that the time needed to reach of the conductivity peak is smaller and the rate of initial conductivity growth is higher when temperature is higher.

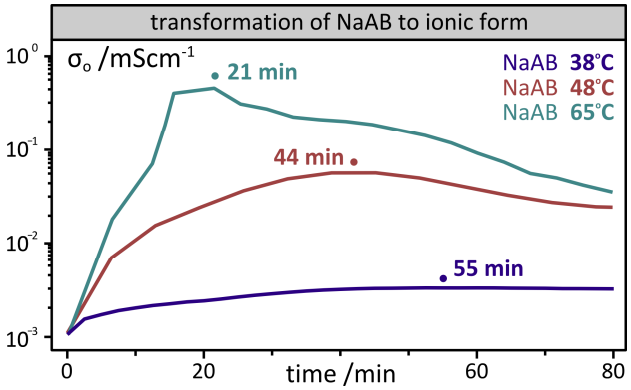

Fig. S3. Conductivity evolution in time for NaAB samples during isothermal EIS measurements at three different temperatures.

4. Comparison of TGA/DSC experiments carried out with 10 K/min and 1 K/min:

We observe emission of hydrogen significantly contaminated with ammonia. To determine if the processes of hydrogen and ammonia evolution are independent we performed TGA/DSC measurements with two scanning rates: 10 K/min and 1 K/min. We observe ammonia evolution as a separate process preceding evolution of hydrogen for all investigated alkali amidoboranes. At 1 K/min experiment hydrogen evolution region is marked with solid gray, ammonia evolution is marked with striped field.

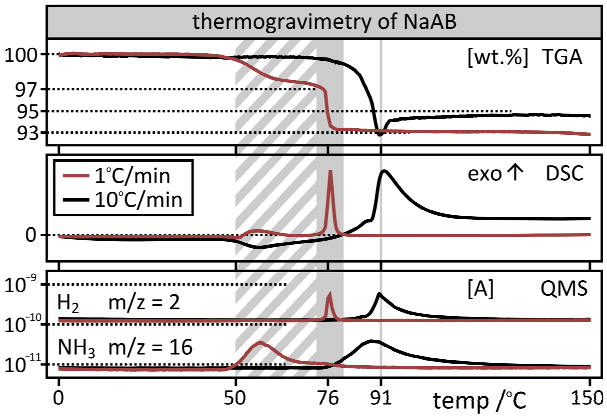

Fig. S4.1. Comparison of TGA/DSC experiments with 10 K/min and 1 K/min scanning rate of NaAB sample.

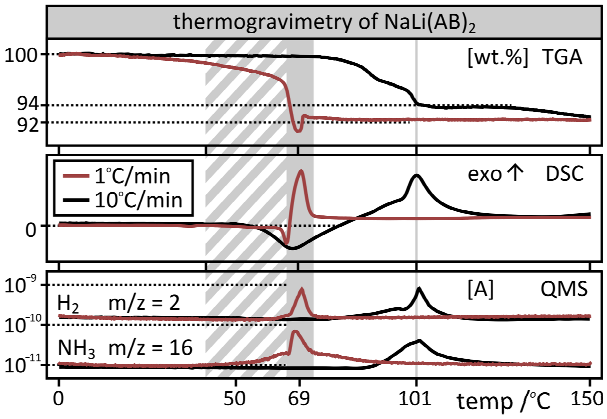

Fig. S4.3. Comparison of TGA/DSC experiments with 10 K/min and 1 K/min scanning rate of $NaLi(AB)_2$ sample.

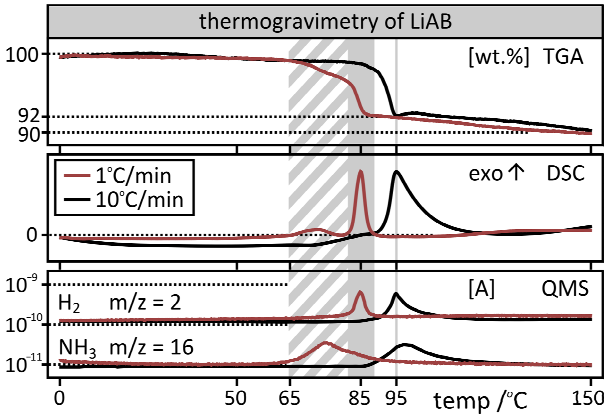

Fig. S4.2. Comparison of TGA/DSC experiments with 10 K/min and 1 K/min scanning rate of LiAB sample.

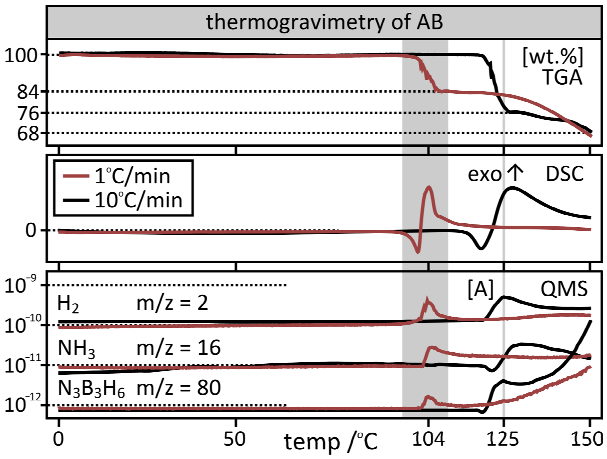

Fig. S4.4. Comparison of TGA/DSC experiments with 10 K/min and 1 K/min scanning rate of AB sample.

5. Comparison of FTIR spectra of thermally treated and aged samples.

To check what is the effect ammonia evolution we collected FTIR spectra of fresh amidoboranes heated to c.a. 50°C. Decomposition over 100°C was also monitored. We observe that thermal decomposition and spontaneous decomposition might follow the same scenario – for confirmation we collected series of spectra of aged samples.

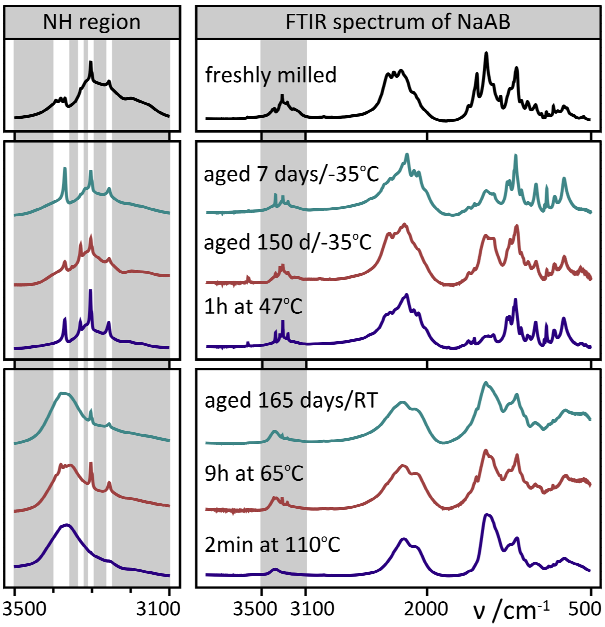

Fig. S5.1. Comparison of FTIR spectra of thermally treated and aged samples of NaAB.

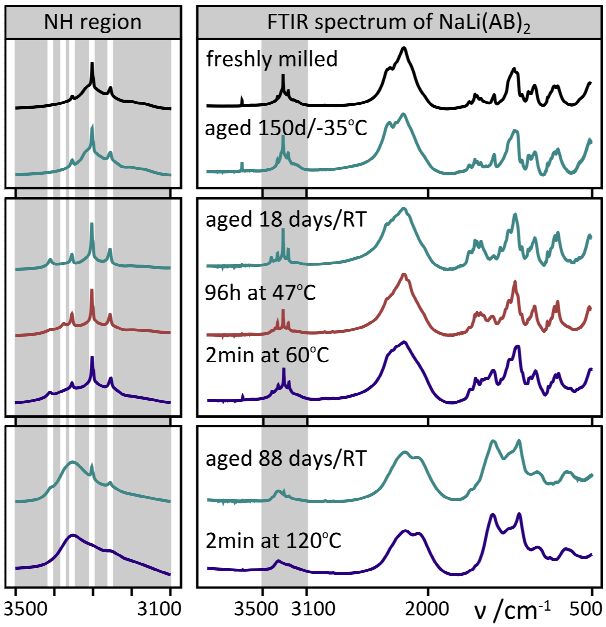

Fig. S5.3. Comparison of FTIR spectra of thermally treated and aged samples of $NaLi(AB)_2$

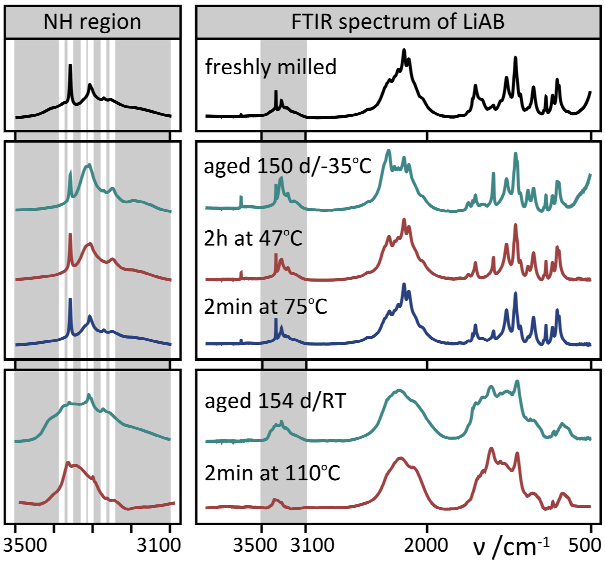

Fig. S5.2. Comparison of FTIR spectra of thermally treated and aged samples of LiAB.

6.1. Table of IR absorption bands of NaAB

Table S6.1. Absorption bands detected in IR spectra (wavenumber [cm^{-1}]) of NaAB at elevated temperature and after aging. Absorption bands of fresh AB, LiAB and $NaLi(AB)_2$ at RT are shown for comparison. Assignment of the bands for AB is according to J. Baumann *et al.*, *Thermochim. Acta*, **430** (2005) 430. (ν = stretching, δ = deformation: bending and torsional modes).

Band	fresh at room temperature			NaAB						
	AB	LiAB	$NaLi(AB)_2$	fresh/RT	7d/-35°C	150d/-35°C	1h/47°C	165d/RT	9h/64°C	2m/110°C
ν(NH)				**3393 vw**						
				3380 vw					**3380 vw**	
		3370 sh		**3369 vw**	**3369 m**	**3370 m**	**3369 m**	**3352 w**	**3365 w**	**3365 w**
		3359 m	**3354 w**			**3351 vw**				
				3329 vw	3329 vw	3329 w	3329 m			
	3311 vs	3310 w	3303 m	3303 m	3303 m	3303 m	3303 s	3303 vw	3303 w	
	3253 vs	3273 vw	3256 w	3256 w	3256 w	3256 w	3256 m	3256 vw	3256 vw	
	3196 s	3251 vw	3215 sh	3200 vw	3200 sh	3199 vw	3200 sh			
		3185 sh	3180 sh							
ν(BH)		2515 sh			2380 sh		2360 sh			
	2347 vs	2326 m	2355 sh	2340 s	2326 s	2337 s	2324 s		2340 sh	
	2289 s	2280 sh	2328 s	2289 s	2280 sh	2282 s	2280 sh		2280 sh	
		2245 s	2275 sh	2224 s		2225 vs				
		2194 vs	2202 vs		2208 vs	2197 vs	2205 sh	2202 vs	2209 vs	2197 s
					2174 vs	2180 vs	2175 vs			
	2118 m	2152 s	2140 sh	2120 sh	2110 s	2120 sh	2110 s	2093 s		2100 sh
		2035 sh	2025 sh	2065 sh	2067 s	2065 sh	2068 s			
ν(BN)				1448 vs	1453 s	1454 s	1431 w	1401 vs	1449 vs	1448 vs
	1363 s	1381 w	1382 m	1385 m	1382 s	1391 s	1384 w	1380 sh	1380 sh	1380 sh
δ(NH)	1611 m	1605 sh	1609 vw	1608 w	1611 w	1606 w	1611 w	1600 sh	1605 sh	1600 sh
		1570 w	1557 w							
		1544 m	1539 w	1532 s	1558 w	1557 w	1557 w	1530 sh	1536 m	1530 sh
		1495 sh	1505 vw							
δ(BH)		1315 sh	1315 sh	1317 m					1315 m	
		1261 s		1260 sh	1261 m	1260 sh	1259 s			
			1245 sh	1232 m	1240 m	1234 s	1239 s	1240 sh	1238 m	1230 sh
			1199 vs	1198 vs	1198 s	1198 s	1199 s	1195 sh	1195 sh	
		1180 vs	1185 sh							
	1163 vs	1165 sh	1177 sh	1173 s	1183 vs	1173 vs	1183 vs	1165 vs	1165 vs	1168 m
		1135 m	1130 w	1129 w	1132 m	1134 m	1133 m		1130 sh	
	1067 s	1065 sh	1071 m	1074 w	1072 w	1072 m	1073 w		1075 sh	
			1055 sh				1056 w			
		1016m	1014 m	999 w	998 m	996 w	999 w	1002 m	997 m	1000 w
other		920 vw	915 vw	922 vw	921 w	921 vw	921 w			
		902 w	895 w	901 w	901 m	900 w	901 m		900 w	
			865 sh	880 vw				873 vw		879 vw
		842 w	834 m	837 w	830 w	830 w	830 w	824 vw	838 w	
		800 m	806 m	797 w		796 vw				793 w
		784 m		742 w	744 m	742 m	744 m	728 m	717 m	739 w

6.2. Table of IR absorption bands of LiAB

Table S6.2. Absorption bands detected in IR spectra (wavenumber [cm^{-1}]) of LiAB at elevated temperature and after aging. Absorption bands of fresh AB, NaAB and $NaLi(AB)_2$ at RT are shown for comparison. Assignment of the bands for AB is according to J. Baumann *et al.*, *Thermochim. Acta*, **430** (2005) 430. (ν = stretching, δ = deformation: bending and torsional modes).

Band	fresh at room temperature			LiAB					
	AB	NaAB	$NaLi(AB)_2$	fresh/RT	150d/-35°C	1h/47°C	2m/75°C	154d/RT	2m/110°C
ν(NH)		**3393 vw**							
		3380 vw							
		3369 vw		**3370 sh**					**3374 vw**
			3354 w	**3359 m**	**3360 m**	**3359 m**	**3359 m**	**3359 w**	
		3329 vw			3315 sh	3315 sh	3315 sh		
	3311 vs	3303 m	3303 m	3310 w	3310 m	3308 m	3310 w	3310 m	3310 vw
	3253 vs	3256 w	3256 w	3273 vw		3275 sh	3273 vw	3273 m	
	3196 s	3200 vw	3215 sh	3251 vw	3251 w	3251 w	3251 vw	3250 sh	3250 sh
			3180 sh	3185 sh	3196 w	3185 sh	3185 sh		
ν(BH)				2515 sh	2515 sh	2515 sh	2515 sh		
			2355 sh		2360 sh	2360 sh	2365 sh		
	2347 vs	2340 s	2328 s	2326 m	2333 vs	2330 s	2326 s	2340 sh	2340 sh
	2289 s	2289 s	2275 sh	2280 sh	2281 s	2280 sh	2275 sh	2280 sh	
		2224 s	2202 vs	2245 s	2246 s	2244 s	2246 s	2245 vs	2223 vs
				2194 vs	2194 vs	2194 vs	2194 vs	2195 sh	
	2118 m	2120 sh	2140 sh	2152 s	2150 vs	2151 vs	2151 vs	2110 sh	2110 sh
		2065 sh	2025 sh	2035 sh	2035 sh	2035 sh	2036 sg		
ν(BN)		1448 vs							
	1363 s	1385 m	1382 m	1381 w	1380 s	1380 m	1380 w	1400 vs	1401 vs
δ(NH)	1611 m	1608 w	1609 vw	1605 sh	1607 w	1606 w	1605 sh	1605 sh	
			1557 w	1570 w	1571 w	1570 sh	1571 vw	1570 m	1570 sh
		1532 s	1539 w	1544 m	1544 m	1544 m	1544 w	1537 m	1540 sh
			1505 vw	1495 sh	1475 vw		1480 sh	1480 sh	1480 sh
δ(BH)		1317 m	1315 sh	1315 sh	1315 sh			1315 s	1318 s
		1260 sh		1261 s	1261 s	1262 s	1261 s	1259 s	
		1232 m	1245 sh						
		1198 vs	1199 vs						
			1185 sh	1180 vs	1179 vs	1179 vs	1179 vs		
	1163 vs	1173 s	1177 sh	1165 sh		1165 sh	1165 sh	1164 vs	1164 vs
		1129 w	1130 w	1135 m	1136 w	1136 w			
	1067 s	1074 w	1071 m	1065 sh	1066 m	1065 w	1065 vw		
			1055 sh					1045 m	1024 m
		999 w	1014 m	1016m	1015 m	1015 m	1016 m	1011 m	
other		922 vw	915 vw	920 vw	921vw	921 vw	920 vw		
		901 w	895 w	902 w	902 w	902 w	902 w		
		880 vw	865 sh						
		837 w	834 m	842 w	842 w	843 w	843 w	829 w	840 w
		797 w	806 m	800 m	799 m	800 m	800 m		
		742 w		784 m	783 m	783 m	783 m	754 m	749 m

6.3. Table of IR absorption bands of $NaLi(AB)_2$

Table S6.3. Absorption bands detected in IR spectra (wavenumber [cm^{-1}]) of $LiNa(AB)_2$ at elevated temperature and after aging. Absorption bands of fresh AB, LiAB and NaAB at RT are shown for comparison. Assignment of the bands for AB is according to J. Baumann *et al.*, *Thermochim. Acta*, **430** (2005) 430. (ν = stretching, δ = deformation: bending and torsional modes).

Band	fresh at room temperature			$NaLi(AB)_2$						
	AB	LiAB	NaAB	fresh/RT	150d/-35°C	18d/RT	96h/47°C	2m/60°C	88d/RT	2m/110°C
ν(NH)			**3393 vw**			**3410 vw**	**3410 vw**	**3410 vw**		
			3380 vw							
		3370 sh	**3369 vw**				**3376 vw**			
		3359 m		**3354 w**	**3354 w**	**3354 w**	**3354 w**	**3354 w**	**3352 w**	**3351 w**
			3329 vw							
	3311 vs	3310 w	3303 m	3303 m	3303 m	3303 m	3303 m	3303 m	3303 vw	3305 sh
	3253 vs	3273 vw	3256 w	3256 w	3256 w	3256 w	3256 w	3256 w	3256 vw	3255 vw
	3196 s	3251 vw	3200 vw	3215 sh	3215 sh	3210 sh	3210 sh	3205 sh	3200 sh	3200 sh
		3185 sh		3180 sh	3180 sh					
ν(BH)		2515 sh								
				2355 sh	2350 sh	2359 s	2360 sh	2355 sh		
	2347 vs	2326 m	2340 s	2328 s	2336 vs		3325 sh	2315 sh		2320 sh
	2289 s	2280 sh	2289 s	2275 sh	2275 s		2270 sh	2275 sh	2270 sh	2270 sh
		2245 s	2224 s	2202 vs	2211 vs	2210 vs	2206 vs	2209 vs	2202 s	2197 s
		2194 vs								
	2118 m	2152 s	2120 sh	2140 sh	2140 sh		2165 vs		2093 s	2081 s
		2035 sh	2065 sh	2025 sh	2025 sh					
ν(BN)			1448 vs				1470 sh	1461 m		
	1363 s	1381 w	1385 m	1382 m	1382 m	1384 vw	1400 m	1397 m	1401 vs	1401 vs
δ(NH)	1611 m	1605 sh	1608 w	1609 vw	1610 vw	1606 w	1605 sh	1605 w	1605 vw	1605 sh
		1570 w		1557 w	1558 w	1557 m	1557 m	1558 m	1560 sh	1560 sh
		1544 m	1532 s	1539 w	1538 w	1538 m	1537 m	1540 m		
		1495 sh		1505 vw	1505 vw	1502 m	1505 m	1500 m		
δ(BH)		1315 sh	1317 m	1315 sh		1326 w	1317 vw	1323 vw	1325 sh	
		1261 s	1260 sh		1275 sh		1275 sh			
			1232 m	1245 sh	1245 sh	1247 s	1244 m	1242 s	1250 sh	1250 sh
			1198 vs	1199 vs	1199 vs	1198 vs	1198 vs	1198 vs	1200 sh	
		1180 vs		1185 sh	1189 vs	1189 vs	1190 vs	1187 vs		
	1163 vs	1165 sh	1173 s	1177 sh	1175 sh		1170 sh	1173 vs	1165 vs	1162 vs
		1135 m	1129 w	1130 w	1131 w	1130 w	1131 m	1130 sh		
	1067 s	1065 sh	1074 w	1071 m	1067 m	1073 w	1070 sh	1070 w		
				1055 sh	1055 sh	1055 w	1055 sh	1060 w		1070 sh
		1016m	999 w	1014 m	1013 m	1013 m	1013 m	1013 m	1002 m	996 m
other		920 vw	922 vw	915 vw	915 vw	915 vw	916 vw	915 vw		
		902 w	901 w	895 w	895 w	896 w	896 w	896 w		
			880 vw	865 sh		863 vw	865 sh	865 sh	873 vw	881 w
		842 w	837 w	834 m	830 m	830 m	831 m	831 m	824 vw	
		800 m	797 w	806 m	802 m	803 m	803 m	803 m		
		784 m	742 w						728 m	733 m

7. XRD study of thermal decomposition of bimetallic lithium-sodium amidoborane

To check what is the effect ammonia evolution on the crystal structure of the residue we collected XRD diffractograms of freshly prepared amidoboranes heated to *ca.* 50°C (at this temperature transformation to ionic phase is already quite advanced and NH_3 is partly desorbed). Decomposition around 100°C was also monitored. We observe after short heating at c.a. 50°C amidoboranes largely remain crystalline (scanning speed > 1°/min), while further heating to 70°C (20°C below hydrogen evolution) results in amorphisation of the samples. It can be anticipated that small fraction of the samples may become amorphous even at 50°C.

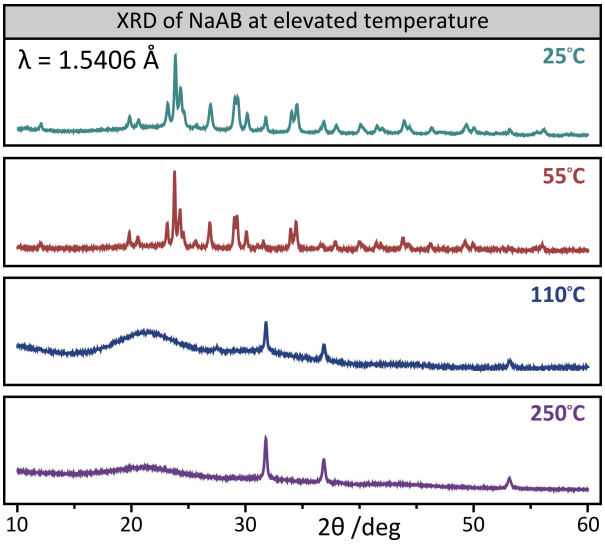

Fig. S7.1. Comparison of diffrectograms collected during thermal decomposition of NaAB sample.

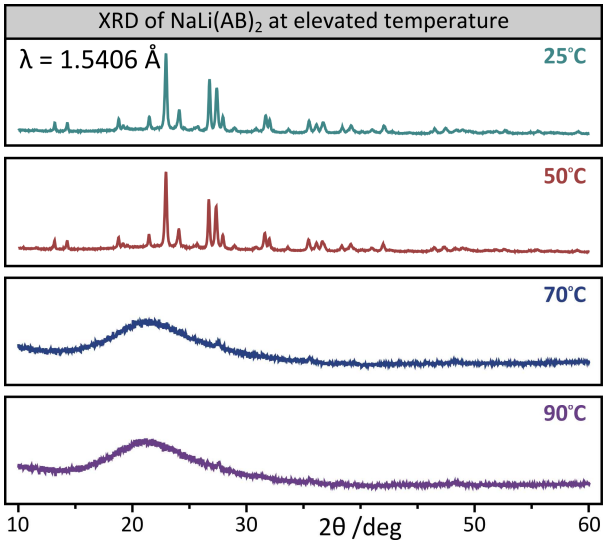

Fig. S7.2. Comparison of diffrectograms collected during thermal decomposition of $NaLi(AB)_2$ sample.

8. Solid state ^{1}H NMR and ^{11}B NMR study of alkali metal amiodoboranes

Table S8. Solid state MAS NMR spectra were collected for fresh NaAB, LiAB and $NaLi(AB)_2$ and the samples heated to 50°C and cooled down to room temperature, to monitor changes associated with the transition to ionic form. At 50°C transformation to ionic phase is already quite advanced and NH_3 is partly desorbed. Small but systematic downshift of the chemical shift in the ^{11}B spectra is observed (by *ca.* 1–2 ppm) as well as considerable downshift of the signals seen in the ^{1}H spectra.

	NaAB		LiAB		$NaLi(AB)_2$	
	fresh	50°C	fresh	50°C	fresh	50°C
^{11}B NMR	–20.5 ppm +21.0 ppm	–21.5 ppm +20.0 ppm	–20.6 ppm +29.5 ppm	–22.4 ppm +27.0 ppm	–20.7 ppm +24.0 ppm	–20.6 ppm +26.2 ppm
^{1}H NMR	–0.2 ppm +2.6 ppm +5 ppm (sh)	– – –	–0.2 ppm +3 ppm (sh)	–2.1 ppm +3 ppm (sh)	–0.5 ppm +0.2 ppm +5 ppm (sh)	–2.2 ppm +4 ppm (sh)

9. Attempts of pre-desorption of NH_3: isothermal heating of NaAB at 48°C and 60°C.

We tried to completely desorb NH_3 from a freshly synthesized NaAB to prepare a novel material which would evolve pure H_2. Samples of NaAB were preheated in a thermostat at 47°C for 2h and 48h. The sample preheated for 2h starts to evolve NH_3 already at 35°C indicating presence of the "ionic phase", but apart from that its TGA profile looks very similar to the profile of freshly prepared NaAB (Fig.S9.1). The sample preheated for 48h is different from that preheated for 2h, but it still evolves some NH_3 (Fig.S9.2). Therefore, we tried to desorb NH_3 during isothermal TGA measurement at 60°C for 2 hours, followed by full heating scan. However, small quantities of NH_3 were still desorbed together with H_2 at *c.a.* 80°C.

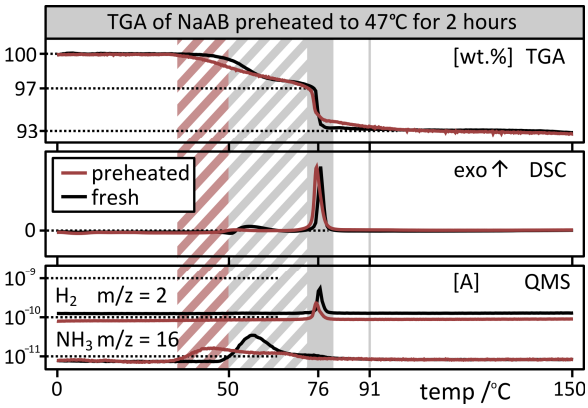

Fig. S9.1. Comparison of TGA/DSC profiles of freshly prepared and preheated NaAB with scanning rate 1K/min. NaAB was preheated at 47°C for 2 hours. Shift of NH_3 evolution onset is marked with red striped field.

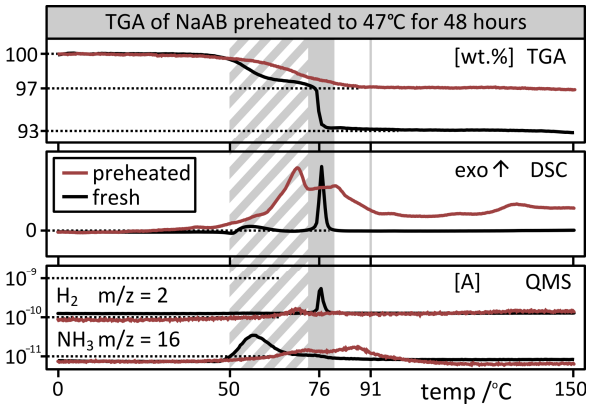

Fig. S9.2. Comparison of TGA/DSC profiles of freshly prepared and preheated NaAB with scanning rate 1K/min. NaAB was preheated at 47°C for 48h.

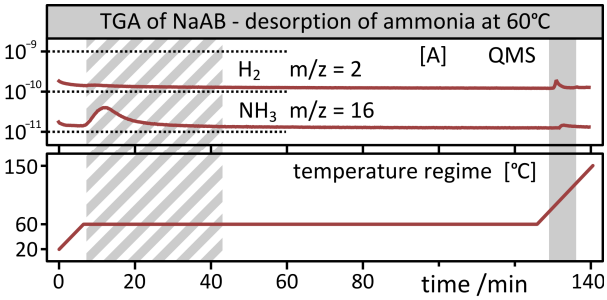

Fig. S9.3. Results of a TGA experiment with an attempt of desorbing NH_3 from NaAB during an isothermal scan at 60°C for 2 hours followed by heating with scanning rate of 1K/min.

10. Heat capacity measurements and low temperature XRD study of NaAB.

We observe a characteristic lambda transition at *ca.* –50°C when measuring heat capacity of NaAB in the range from room temperature down to 10K. The observed transition is reversible with no hysteresis. The temperature at which the transition takes place is similar to the temperature of crystallographic phase transition of AB precursor (225 K or –48 °C according to: N. J. Hess et al., J. Phys. Chem. A 113 (2009) 5723-5735). To elucidate the origin of the observed lambda transition we have collected low temperature XRD patterns (–60°C, –160°C, –170°C) of NaAB. However, we do not observe any high- or low-T AB forms in the XRDP (the only new reflections that appear after cooling represent ice which cover a quartz capillary during low temperature measurements). In addition, the integrated heat of the lambda peak strongly varies from sample to sample (22–211 J mol^{-1} NaAB), while the heat associated with the crystallographic phase transition of AB equals 1290 J mol^{-1} (O. Palumbo et al., J. Alloys Comp. 5095 (2011) 5709-5713). This means that if AB was responsible for the observed lambda peak, its content in the sample would be around 1.5–15 mol %; the latter number seems to be impossible at first, since as much as 15 mol % AB would immediately be seen in XRD pattern. One possible explanation of this discrepancy is that some AB might be generated during loading of the sample for specific heat measurement; exposure of NaAB to atmosphere results in partial hydrolysis yielding AB (K. Fijalkowski et al., J. Mater. Chem. 19 (2009) 2043-2050). AB is not seen in XRD patterns since the sample studied with thermal resolution has not been subjected to atmosphere at all (quartz capillary was sealed).

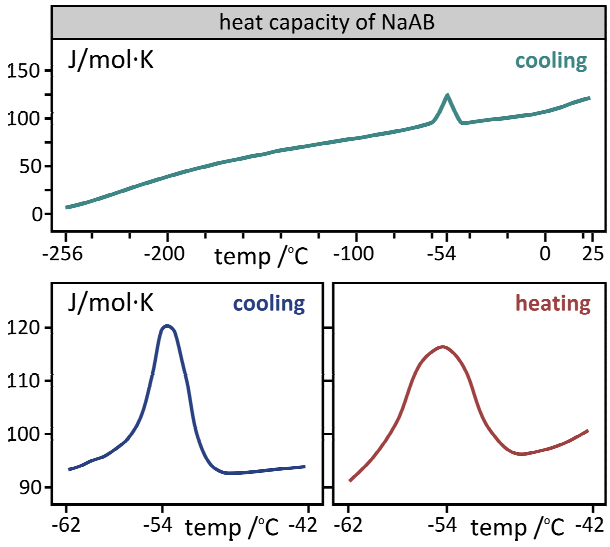

Fig. S10.1. Results of heat capacity measurement of NaAB sample with visible lambda transition peak at –54°C.

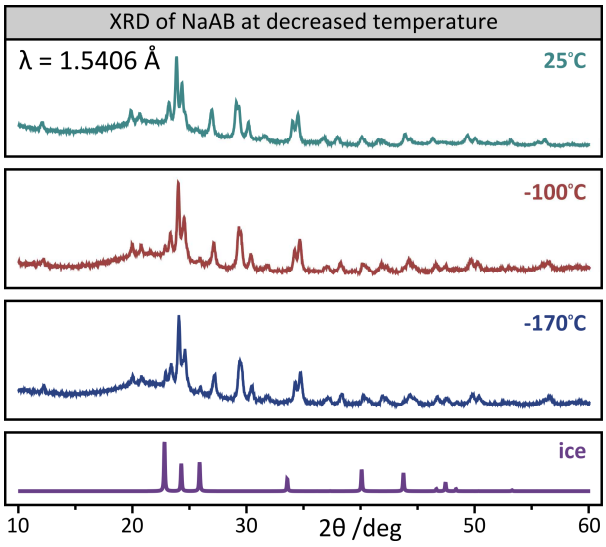

Fig. S10.2. Comparison of diffractograms collected while cooling NaAB sample. In the bottom frame pattern of hexagonal ice is shown.